Brazilian Journal
of Chemical
Engineering

ISSN 0104-6632
Printed in Brazil
www.abeq.org.br/bjche

Vol. 33, No. 02, pp. 287 - 296, April - June, 2016
dx.doi.org/10.1590/0104-6632.20160332s20150234

NUMERICAL SIMULATION OF THE INCOMPRESSIBLE TURBULENT FLOW OF A BINARY MIXTURE OF AIR-WATER VAPOR: APPLICATIONS IN DRYING PROCESS

P. S. B. Zdanski[1*] and D. Silva[2]

[1]State University of Santa Catarina, UDESC, Department of Mechanical Engineering, Campus Universitário Avelino Marcante s/n, Zona Industrial Norte, 89219-710, Joinville - SC, Brazil.
E-mail: paulo.zdanski@udesc.br
[2]Tupy S.A, Joinville - SC, Brazil.

(Submitted: April 15, 2015 ; Accepted: May 6, 2015)

Abstract - The present work deals with numerical simulation of the incompressible turbulent flow of a binary mixture air-water vapor inside channels. Calculations are performed using the RANS (Reynolds Average Navier-Stokes Equations) formulation in addition to the standart k-ε turbulence model. The mathematical model is discretized by a finite difference scheme, being adopted second order accurate expressions for both convection and diffusion terms. The mesh arrangement is collocated and artificial dissipation terms are added to control the odd-even decoupling problem. The numerical scheme is applied to solve the flow of a binary mixture of air-water vapor inside plane channels and sudden expansions. The validation performed indicates that the present method reproduces satisfactorily the literature data for both concentration profiles and Sherwood number. Furthermore, the parametric analysis performed indicates that the drying process (wall mass flux) is very sensitive to the flow parameters investigated, i.e., inlet flow velocity and channel expansion ratio.
Keywords: Binary mixture; Turbulent flow; Numerical analysis; Finite difference method.

INTRODUCTION

The turbulent flow of binary mixtures occurs in practical problems of the chemical and mechanical engineering areas. In the convective drying process, water vapor is removed from moist objects (e.g. wood, food, etc.), being transported by the hot air stream. It is important to mention that convective drying is the most used method in agricultural, food, paper and timber processing industries (Mohan and Talukdar, 2010). In general applications, convective drying of moist objects conjugates heat and mass transfer both inside the solid and in the flowing medium (Vaz Jr *et al*., 2013). The understanding of the related physics of the problem is important for industrial process control.

The literature works dealing with this topic are increasing, mainly in the numerical analysis area. Younsi *et al*. (2010) adopted the commercial software ANSYS-CFX to solve numerically the turbulent flow of a binary mixture in a wood dry kiln. The authors compared the numerical results with experimental data aiming at validating the simulation. Kadem *et al*. (2011) solved numerically the conjugate heat and mass transfer problem in a convective wood dry kiln using the commercial software FEMLAB. The mathematical model adopted by the authors to solve the flow of a binary mixture is the Navier-

*To whom correspondence should be addressed

Stokes equations subjected to laminar flow conditions. The results obtained indicate a correlation between drying rate in the solid and the flow behaviour. In a similar route, Lamnatou *et al*. (2009) studied numerically the drying process of a moist object (a porous sliced wood) subjected to incompressible laminar flow of a binary mixture inside a channel. The authors analysed the effects of two flow configurations, and the results indicated that using the upstream flow divider device produced a higher mass transfer rate at the surface of the moist object (enhancing the drying rate).

In other interesting practical applications, some literature works solve the flow of a binary mixture to study both the environmental problem of pollutant dispersion and the chemical corrosion of metallic surfaces (Xiong *et al*., 2014; Lateb *et al*., 2013; Arellano *et al*., 2013; Arellano and Rivera, 2014). The aforementioned works adopted the numerical methodology to study practical aspects of the problem, i.e., to estimate the mass flux of the chemical component on the surface, the concentration of the pollutant between the buildings in a city, etc.

The present work deals with the 2D numerical simulation of turbulent flow of a binary mixture (air-water vapor) aiming to study some aspects of the convective drying process. The numerical scheme applied by the authors was originally proposed for solving turbulent Newtonian flows (Zdanski *et al*. 2004). The present methodology was also applied successfully to solve non-Newtonian polymer melt flows inside channels (Zdanski *et al*., 2008; Zdanski and Vaz Jr., 2011). Therefore, the present work performs an extension of the author's methodology for solving turbulent flows of binary mixtures, including the solution of the concentration equation. The results obtained indicate that the present method reproduces satisfactorily the literature data for both concentration profiles and Sherwood number. Furthermore, the parametric analysis performed shows that the drying process (mass flux at the channel walls) is dramatically affected by the flow parameters investigated, i.e., inlet flow velocity and channel expansion ratio.

THEORETICAL FORMULATION

Governing Equations

The mathematical model employed corresponds to the classical Reynolds Averaged Navier-Stokes Equations (RANS) together with the Boussinesq eddy viscosity approximation. Within this framework, the mass, linear momentum, energy and chemical species conservation laws are solved to obtain the average velocities, pressure, temperature and concentration profiles of the flow. In cartesian tensor notation, the equations are given by (Kays and Crawford, 2005):

$$\frac{\partial\left(\rho\overline{u}_i\right)}{\partial x_i}=0\,, \tag{1}$$

$$\frac{\partial\left(\rho\overline{u}_i\right)}{\partial t}+\frac{\partial\left(\rho\overline{u}_j\overline{u}_i\right)}{\partial x_j}=-\frac{\partial\overline{p}_e}{\partial x_i}+\frac{\partial}{\partial x_j}\left[\mu_e\left(\frac{\partial\overline{u}_i}{\partial x_j}+\frac{\partial\overline{u}_j}{\partial x_i}\right)\right], \tag{2}$$

$$\frac{\partial\left(\rho c_p\overline{T}\right)}{\partial t}+\frac{\partial\left(\rho\overline{u}_i c_p\overline{T}\right)}{\partial x_i}=\frac{\partial}{\partial x_i}\left(k_e\frac{\partial\overline{T}}{\partial x_i}\right), \tag{3}$$

$$\frac{\partial\left(\overline{C}\right)}{\partial t}+\frac{\partial\left(\overline{u}_i\overline{C}\right)}{\partial x_i}=\frac{\partial}{\partial x_i}\left(D_{AB_e}\frac{\partial\overline{C}}{\partial x_i}\right), \tag{4}$$

where $\mu_e=\mu+\mu_T$, $k_e=k+k_T$ and $D_{AB_e}=D_{AB}+D_{AB_T}$ are the effective diffusion coeficients, and $\overline{p}_e=\overline{p}+2/3\rho\kappa$ is the effective pressure. In the preceding expressions, μ_T, k_T and D_{AB_T} are the turbulent diffusion coeficients, being determined by the standard two-equation $\kappa-\varepsilon$ turbulence model. In the present model, two differential equations are solved for the turbulence kinetic energy (κ) and its dissipation rate (ε), i.e.,

$$\begin{aligned}&\frac{\partial\left(\rho\kappa\right)}{\partial t}+\frac{\partial\left(\rho\overline{u}_j\kappa\right)}{\partial x_j}=\\&\frac{\partial}{\partial x_j}\left[\frac{\mu_T}{\sigma_k}\frac{\partial\kappa}{\partial x_j}\right]+\mu_T\left(\frac{\partial\overline{u}_i}{\partial x_j}+\frac{\partial\overline{u}_j}{\partial x_i}\right)\left(\frac{\partial\overline{u}_i}{\partial x_j}\right)-\rho\varepsilon\end{aligned}\,, \tag{5}$$

$$\begin{aligned}\frac{\partial\left(\rho\varepsilon\right)}{\partial t}+\frac{\partial\left(\rho\overline{u}_j\varepsilon\right)}{\partial x_j}=&\frac{\partial}{\partial x_j}\left[\frac{\mu_T}{\sigma_\varepsilon}\frac{\partial\varepsilon}{\partial x_j}\right]\\&+C_{\varepsilon1}\frac{\varepsilon}{\kappa}\mu_T\left(\frac{\partial\overline{u}_i}{\partial x_j}+\frac{\partial\overline{u}_j}{\partial x_i}\right)\left(\frac{\partial\overline{u}_i}{\partial x_j}\right)\\&-C_{\varepsilon2}\rho\frac{\varepsilon^2}{\kappa}\end{aligned}, \tag{6}$$

the turbulent eddy viscosity being calculated by:

$$\mu_T=C_\mu\rho\frac{\kappa^2}{\varepsilon}\,. \tag{7}$$

The constants appearing in the preceding equations are empirically determined (Launder and Spalding, 1974), i.e.,

$$C_\mu = 0.09\,,\ C_{\varepsilon 1} = 1.44\,,\ C_{\varepsilon 2} = 1.92\,,$$
$$\sigma_\kappa = 1.0\,,\ \sigma_\varepsilon = 1.3\,. \tag{8}$$

The turbulent diffusion coeficients in the energy and chemical species equations are obtained by using the analogy between linear momentum, heat and mass diffusion processes through the definition of the turbulent Prandtl and Schmidt numbers (Kays and Crawford, 2005),

$$k_T = \frac{\mu_T c_p}{\mathrm{Pr}_T}\,, \tag{9}$$

$$D_{AB_T} = \frac{\mu_T}{\rho Sc_T}\,. \tag{10}$$

The turbulent Prandtl and Schmidt numbers are assumed to be constants, being adopted common values for engineering calculations $\mathrm{Pr}_T = Sc_T = 0.9$ (Kays and Crawford, 2005). It is worth to mention that the standard $\kappa - \varepsilon$ turbulence model is valid only for the fully turbulent region; in the near wall regions the law of the wall for velocity, temperature and concentration profiles is adopted (Launder and Spalding, 1974; Kays and Crawford, 2005; Arpaci and Larsen, 1984).

Numerical Methodology

The mathematical model is discretized with a finite difference scheme, second order accurate formulae being adopted for both the convection and diffusion terms. The mesh arrangement is collocated and artificial dissipation terms are added to control the odd-even decoupling problem. The pressure-velocity coupling strategy employed comprises the solution of the Poisson equation for pressure. The solution procedure follows a pseudo-transient march in time, aiming at the steady-state solution. The present work constitututes an extension of the author's methodology (Zdanski *et al*., 2004; Zdanski *et al*., 2008; Zdanski and Vaz Jr., 2011) for solving turbulent flows of binary mixtures. The main general steps of the present scheme are given in sequence.

The linear momentum, energy and chemical species conservation equations, as well as the turbulence model equations, can be written in a compact form (for a 2D cartesian coordinate system)

$$\frac{\partial Q}{\partial t} + \frac{\partial E}{\partial x} + \frac{\partial F}{\partial y} = S\,, \tag{11}$$

where Q is the vector of conserved variables, E, F and S are the flux vectors containing the convection, diffusion and source terms. The vector Q is expanded in time by Taylor expansion:

$$Q^{m+1} = Q^m + \left(\frac{\partial Q}{\partial t}\right)^{m+1} \Delta t \tag{12}$$

in which m and Δt are the time step and time increment, respectively. Furthermore, from Equation (11) one finds:

$$\frac{\partial Q}{\partial t}^{m+1} = -\left(\frac{\partial E}{\partial x} + \frac{\partial F}{\partial y} - S\right)^{m+1}\,. \tag{13}$$

Solution of Equation (12) requires linearization of vectors E, F and S in terms of vector Q using Taylor expansion and defining the Jacobian matrices at time step m. The resulting equation may be expressed as

$$\left[I + \Delta t\left(\frac{\partial A^m}{\partial x} + \frac{\partial B^m}{\partial y} - J^m\right)\Delta Q^m = -\Delta t\left(\frac{\partial E^m}{\partial x} + \frac{\partial F^m}{\partial y} - S^m\right)\right]\,, \tag{14}$$

where A, B and J are the Jacobian matrices, and $\Delta Q^m = Q^{m+1} - Q^m$ is the variable delta form. In order to reduce the computational effort in the numerical solution of Equation (14), the approximate factorization technique (Beam and Warming, 1978) is introduced. Besides, to reach second order spatial accuracy, the scheme uses a central discretization for both convection and diffusion terms; however, to circumvent the odd-even decoupling problem (Patankar, 1980), artificial dissipation terms are added externally. The final form of the equation is:

$$L_x L_y \Delta Q^m = R_x + R_y\,, \tag{15}$$

where

$$L_x = I + \Delta t\left(\frac{\partial A^m}{\partial x} - \frac{J^m}{2}\right) - \varepsilon_i \left(\Delta x\right)^2 \frac{\partial^2}{\partial x^2}\,, \tag{16}$$

$$L_y = I + \Delta t\left(\frac{\partial B^m}{\partial y} - \frac{J^m}{2}\right) - \varepsilon_i (\Delta y)^2 \frac{\partial^2}{\partial y^2}, \quad (17)$$

$$R_x = -\Delta t\left(\frac{\partial E^m}{\partial x} - \frac{S^m}{2}\right) - \varepsilon_e (\Delta x)^4 \frac{\partial^4 Q^m}{\partial x^4}, \quad (18)$$

$$R_y = -\Delta t\left(\frac{\partial F^m}{\partial y} - \frac{S^m}{2}\right) - \varepsilon_e (\Delta y)^4 \frac{\partial^4 Q^m}{\partial y^4}, \quad (19)$$

I being the identity matrix, ε_i and ε_e the artificial dissipation coefficients and Δx and Δy the nodal distance along the corresponding coordinate axes. Following an ADI (alternating direction implicitly) concept, Equation (15) is solved as a sequence of two one-dimensional problems

$$\Delta Q^m = L_y^{-1}\left[L_x^{-1}\left(R_x + R_y\right)\right], \quad (20)$$

$$Q^{m+1} = Q^m + \Delta Q^m. \quad (21)$$

Finally, it is important to mention that the artificial dissipation coefficients ε_i and ε_e are calibrated numerically and the values found to be adequate were $\varepsilon_i = 0.001$ and $\varepsilon_e = 0.003$. The complete procedure to control the magnitude of the artificial smoothing terms is described by Zdanski *et al*. (2004).

RESULTS AND DISCUSSION

Validation/Verification of the Numerical Solution

This section comprises the validation of the numerical method applied. The flow of a binary mixture in a two-dimensional plane channel was the benchmark problem selected, i.e., the turbulent concentration profiles and the Sherwood number distribution were confronted with literature data (for three meshes). Firstly, in Fig. 1 the dimensions of the geometry are presented, i.e., the channel height h=0.011 m and the channel length L=60 h. The computational meshes adopted in the simulations are uniform with 201 × 31, 301 × 35 and 401 × 41 grid points in the streamwise and cross-sectional directions, respectively. Boundary conditions at the inlet plane are: uniform velocity, temperature and concentration profiles, with the Reynolds number based on the hydraulic diameter equal to 27.480. For this test, the following values were applied: u_i = 18.68 m/s, C_i = 0.00788 kg/m^3 and κ_i = 0.02 $(u_i)^2/2$, with u_i, C_i and κ_i being the inlet velocity, concentration and turbulent kinetic energy, respectively. At the exit section, parabolic conditions (null derivatives) are specified for all the variables, except for pressure, whose variation is considered to be linear. At the solid walls, a constant mass flux of the chemical species (water vapor) is imposed, $No_w^{"}$ = 0.025 kg/m^{2}s.

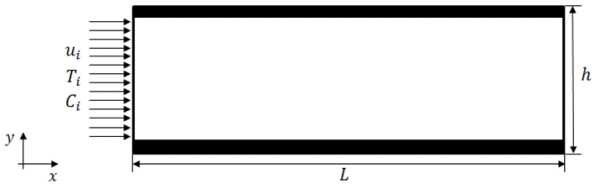

Figure 1: Illustration of the two-dimensional channel with the main dimensions.

Figure 2 shows the computed non-dimensional concentration profiles at the channel exit section (L/h = 60), corresponding to the fully developed flow region. As can be seen in the figure, the results clearly indicate that the numerical scheme reproduces satisfactorily the literature concentration profile for the three meshes tested. The benchmark solution in this case is the classical correlation according to Kader (1981), that was developed to fit the experimental data for fully developed flow regions in plane channels and circular ducts. The non-dimensional concentration is defined as $C^+=(C-C_w)/C,^*$ where $C^*= No_w^{"}/u^*$ and $u^*=C_\mu^{0.5}\kappa^{0.25}$ (u^* being the shear velocity), and the parameter y^+ (non-dimensional distance from the wall) is given by $y^+ = \rho u^* y/\mu$.

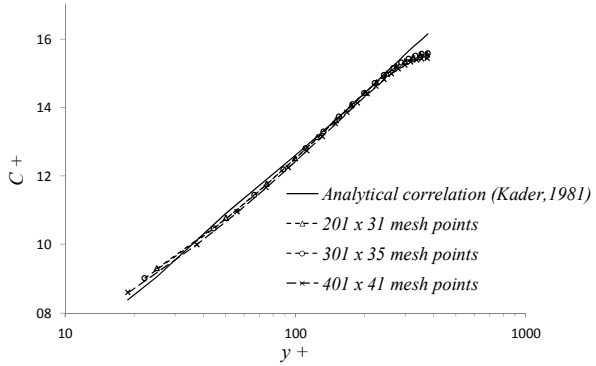

Figure 2: Comparisons between analytical correlation and computations for the concentration profile in the fully developed flow region.

Furthermore, Figure 3 presents the Sherwood number distribution along the channel walls. The Sher-

wood number (*Sh*) expresses the local convective mass transfer coefficient (h_m), i.e.,

$$Sh = \frac{h_m D_h}{D_{AB}}, \tag{22}$$

$$h_m = \frac{-D_{AB}\left.\partial \bar{C} \middle/ \partial y\right|_w}{C_m - C_w}, \tag{23}$$

$$C_m = \frac{\int_A \rho u \bar{C} dA}{\rho u_m A}, \tag{24}$$

where C_m is the bulk concentration of the chemical species, C_w is the concentration at the channel walls, h_m is the local convective mass transfer coefficient, D_h is the hydraulic diameter and u_m is the average velocity in the channel cross section.

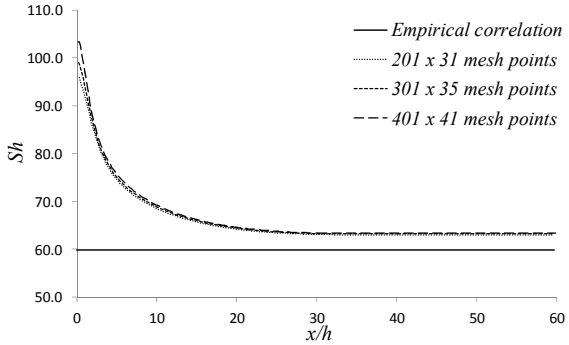

Figure 3: Comparisons between the empirical correlation and computations for the Sherwood number.

The results presented in Figure 3 indicate a good agreement between the numerical solution and the empirical correlation in the fully developed flow region ($x/h \geq 25$), the error being around 6%. It is important to mention that the Sherwood number for the fully developed flow region is obtained from the empirical correlation of Dittus-Boelter (Incropera *et al*., 2007), i.e.,

$$Sh = \frac{h_m D_h}{D_{AB}} = 0.023\,\mathrm{Re}_{Dh}^{0.8}\, Sc^{0.4}, \tag{25}$$

Re_{Dh} and *Sc* being the Reynolds and molecular Schmidt numbers. Finally, it is important to mention that the numerical results obtained with the present scheme (see Figures 2 and 3) are clearly mesh independent.

Flow in a Wood Dry Kiln

A typical convective wood dry kiln comprises various channels that are formed between the wood stacks. The previous numerical results of Possamai (2013) and Zdanski *et al*. (2015), assessing the aerodynamic effects in a dry kiln, have shown that flow inside the channels can be highly non-uniform. Besides, according to the same authors, flow stagnation regions and recirculation zones are typically found in a dry kiln device. Therefore, this section aims at studying the effects of the aforementioned flow characteristics on the drying rate of the wood stack (mass flux in the channel walls).

The geometry adopted in the simulations, along with the flow configuration at the channel entrance section, is shown in Figure 4. A parametric study was performed, i.e., the inlet flow velocity and the incidence angle ($\hat{A}$) were varied to assess the influences on mass transfer at the channel walls. In the present test the boundary conditions were specified similarly to the validation case, except the concentration at the walls that was set to a constant value, C_w = 0.025 kg/m^3, and the inlet flow velocity was varied. The computational mesh adopted in the simulations is uniform with 201 x 31 grid points, the channel dimensions being equal to the validation case.

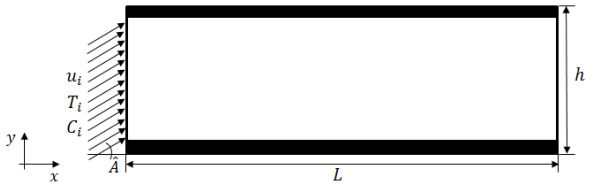

Figure 4: Illustration of the two-dimensional channel with variable flow incidence angle.

Firstly, in order to study the effects of distinct inlet flow velocities on mass flux at the channel walls, parallel flow was considered ($\hat{A}$=0). The flow velocities tested were u_i = 6, 8, 10 and 12 m/s, values typically found in a wood dry kiln (Zdanski *et al*., 2015). The main results are presented in Figure 5, with the convective mass transfer coefficient represented along the channel walls (see the definition of Equation (23)). The analysis of the results clearly indicates that mass flux at the walls is greatly enhanced as the inlet flow velocity varies from 6 to 12 (average increase around 95%). The mass transfer of water vapor is higher at the entrance flow region, reducing to a plateau in the fully developed region (this behaviour is similar to a convective heat transfer phenomenon). Therefore, the main conclusion of the results is that distinct inlet flow velocities affects

drastically the mass transfer at the channel walls (and probably the drying rate of the wood stacks).

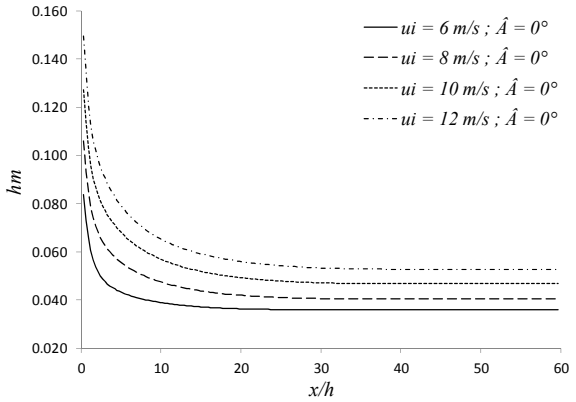

Figure 5: Convective mass transfer coefficient for distinct inlet flow velocities *(Â=0)*.

The results of Figure 6 show the convective coefficient for non-vanishing incidence angle at the channel entrance. It is important to mention that the aforementioned flow topology typically occurs inside a wood dry kiln (Possamai, 2013; Zdanski *et al*., 2015), being worthy of investigation. The entrance velocity u_i was set variable with respect to the incidence angle in order to produce an uniform mass flow of the mixture in the channel for the cases tested ($\hat{A}$=0°,10°, 20°, 30° and 40°), i.e.,

$$\dot{m} = \int_A \rho u dA = cte\,. \tag{26}$$

The results of Figure 6 clearly indicate that mass transfer of the chemical species (water vapor) at the channel walls was enhanced in the entrance flow region (x/h<25) as the flow incidence angle increased.

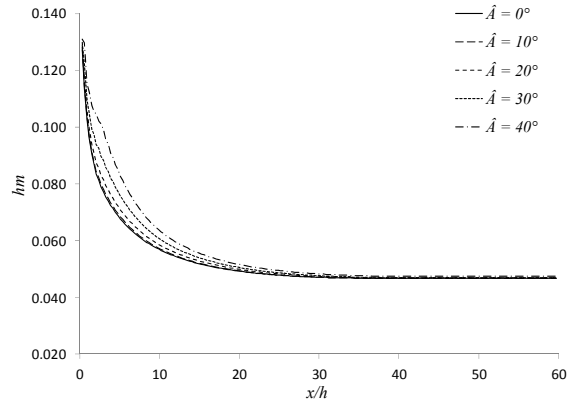

Figure 6: Convective mass transfer coefficient for distinct incidence angles ($\hat{A}$).

The physical scenario is dominated by the stagnation region formed at the channel upper wall, that leads to enhancement in the convective mass transfer process. Otherwise, in the fully developed flow region (x/h>25) the convective coefficient is basically constant (an expected result due to the occurrence of similar velocity profiles in this region).

Finally, in order to conclude this section Figure 7 shows the results for the average Sherwood number along the channel length for $\hat{A}$=10° and 40° and for all velocities tested, i.e.,

$$\overline{h}_m = \frac{\int_{A_s} h_m dA_s}{\int_{A_s} dA_s} \quad \text{and} \quad \overline{Sh} = \frac{\overline{h}_m D_h}{D_{AB}}\,. \tag{27}$$

The results show basically a linear variation between Sherwood and Reynolds numbers. The convective mass transfer enhancement was also observed when the flow presented an incidence angle, this behaviour being related to the stagnation region formed at the upper wall.

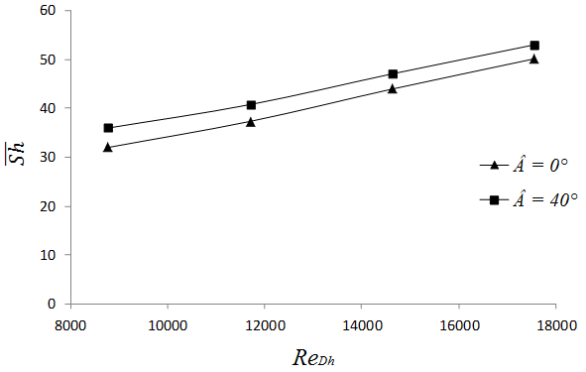

Figure 7: Average Sherwood number as function of Reynolds number for $\hat{A}$=0° and 40°.

Flow in Channels with Sudden Expansion

The results of Zdanski *et al* (2015) show that recirculation regions are formed inside the channels of wood stacks in a dry kiln. Aiming to study the effects of these regions on mass transfer at the walls, the flow in a channel with sudden expansion was idealized. For this test, the boundary conditions adopted are equal to the validation case, except the inlet flow velocity was varied. The geometry is presented in Figure 8, with the channel height h=0.011 m and the channel length L=30 h. The step height s was set variable in a parametric study and the computational

mesh uniform with 901 × 31 grid points in the x and y directions, respectively. The velocity at the inlet section was set as follows: u_i = 16 m/s for the channel with expansion ratio $ER = (h\text{-}s)/(h) = 1/2$; u_i = 12 m/s for ER = 2/3 and u_i = 10 m/s for ER = 5/6. Finally, it is important to mention that u_i was set variable with respect to the expansion ratio in order to produce an uniform mass flow of the mixture in a channel for the cases tested (see Equation (26)).

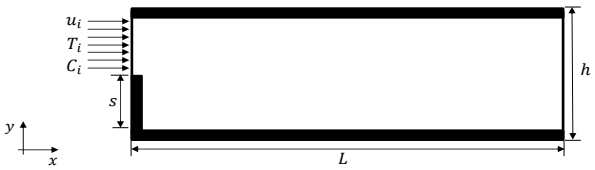

Figure 8: Illustration of the two-dimensional channel with sudden expansion section.

The purpose of this section was to study the effects of the expansion ratio on the mass flux of the chemical species (water vapor) at the solid walls. Figure 9 shows the results for the convective mass transfer coefficient at the lower and upper channel walls for an expansion ratio ER = 1/2. The convective coefficient at the upper wall presents behaviour similar to the plane channel (the maximum value occurs at the entry region). Otherwise, the recirculation zone formed at the stepped wall produces a distinct behaviour on the convective coefficient, i.e., a maximum value near the reattachment point (similar behaviour was obtained for heat transfer results in a back step problem with the effects of turbulence promoters – see Zdanski *et al*., 2015) followed by a sharp decrease towards the exit section.

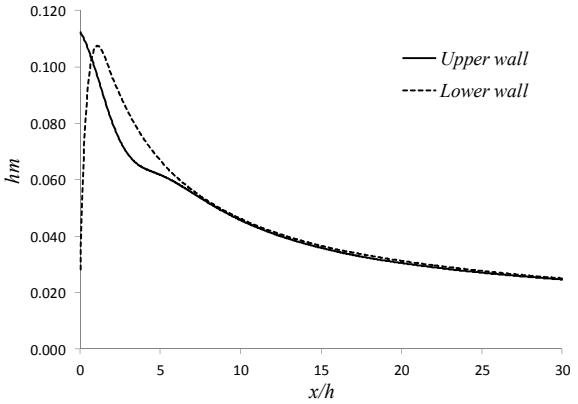

Figure 9: Convective mass transfer coefficient for the channel with expansion ratio ER = 1/2.

Aiming to clarify the physics of the problem, Figure 10 presents the streamlines (flow topology) with the vortex region clearly indentified. It is important to mention that, for the conditions simulated, the reattachment length was around x/s = 4.0 (or x/h = 2.0), and the vortex zone imposed a reduction in the mass transfer near the vertical wall at the entrance section (x/h = 0).

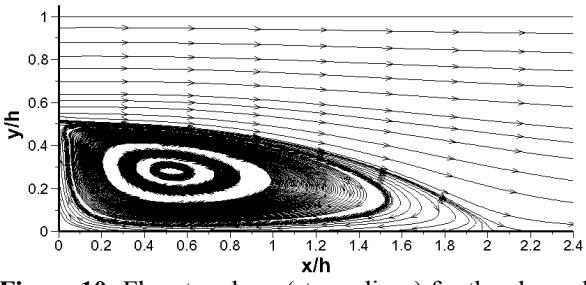

Figure 10: Flow topology (streamlines) for the channel with expansion ratio ER = 1/2.

The effects of the expansion ratio (ER) on mass flux at the channel walls are presented in Figures 11 and 12. The results clearly indicate that the mass fluxes at both walls are reduced in the entry flow region (x/h < 15) with increasing expansion ratio ER. This behaviour may be explained due to the occurrence of lower velocities in this region since the flow passage area was enhanced. Otherwise, the point of maximum value at the lower wall (see Figure 12) displaces towards the entrance section due to reduction in the recirculation region as the expansion ratio was increased (for the cases simulated x/s = 4, but as the step height s decreases, the vortex length also reduces – see Figures 13 and 14). Finally, in the flow region towards the exit section (x/h > 15) the results for the convective coefficient at the lower and upper walls are similar (with minor differences) for all expansion ratios (this is an expected result since the average velocities inside the channels are equal in this region).

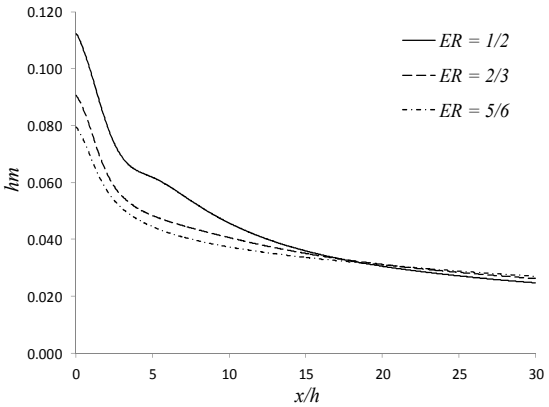

Figure 11: Convective mass transfer coefficient for the upper wall in the channel with variable expansion ratios (ER).

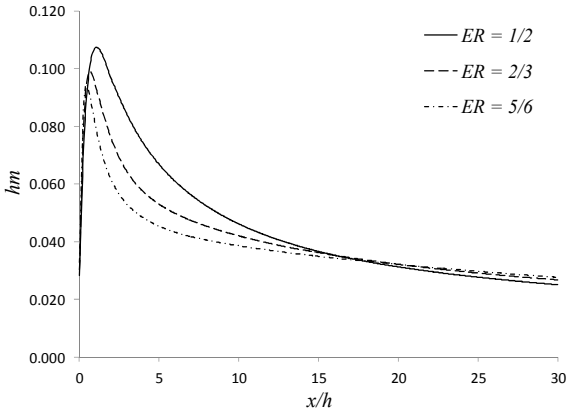

Figure 12: Convective mass transfer coefficient for the lower wall in the channel with variable expansion ratios (*ER)*.

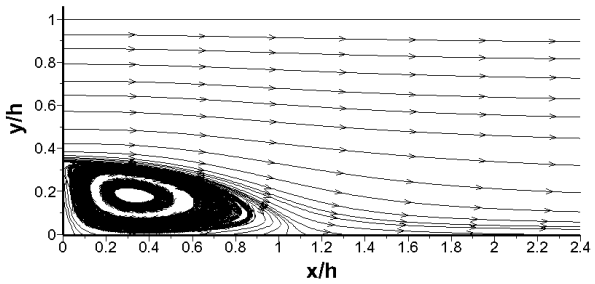

Figure 13: Flow topology (streamlines) for the channel with expansion ratio *ER* = 2/3.

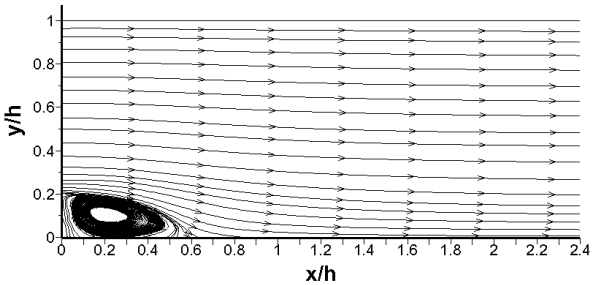

Figure 14: Flow topology (streamlines) for the channel with expansion ratio *ER* = 5/6.

CONCLUSIONS

In this paper a numerical method is presented for solution of the turbulent flow of a binary mixture inside channels. The numerical results obtained indicate that the scheme reproduced satisfactorily the literature data for both concentration profiles and Sherwood number. Furthermore, the numerical solution obtained was clearly mesh independent.

Besides, in the physical analysis performed, the main conclusions are: (i) the parametric study reveals that distinct inlet flow velocities produce drastic effects on the convective mass transfer coefficient. The analysis of the results clearly indicates that mass flux at the walls is highly enhanced as the inlet flow velocity varies from 6 to 12 (an average increase around 95%). Furthermore, the wall mass flux of the chemical species (water vapor) was enhanced in the entrance flow region (x/h<25) as the flow incidence angle increases. The physical scenario is dominated by the stagnation region formed at the channel upper wall, that leads to enhancement of the convective mass transfer process. (ii) The flow in a sudden expansion reveals that the convective coefficient is very sensitive to the expansion ratio *ER*. In the entry flow region the mass flux reduces as the expansion ratio increases. Furthermore, the maximum value for mass flux near the reattachment point displaces towards the vertical wall as a consequence of the reduction of the vortex zone.

NOMENCLATURE

A	Jacobian matrices
$\hat{A}$	incidence angle [°]
A_s	surface area [m^2]
B	Jacobian matrices
$\overline{C}$	average concentration of the chemical component [kg/m^3]
C_i	concentration of the chemical component at the inlet [kg/m^3]
C_m	bulk concentration [kg/m^3]
C_w	concentration of the chemical component at the walls [kg/m^3]
C^+	non-dimensional concentration [-]
c_p	specific heat coefficient [J/kgK]
cte	constant [kg/s]
$C_{\varepsilon 1}, C_{\varepsilon 2}, C_\mu$	turbulence model constants [-]
D_{AB}	molecular diffusion coefficient of chemical species A in B [m^2/s]
D_{ABT}	turbulent diffusion coefficient of chemical species A in B [m^2/s]
D_{ABe}	effective diffusion coefficient of chemical species A in B [m^2/s]
D_h	hydraulic diameter [m]
ER	channel expansion ratio [-]
E, F	Flux vectors
h	channel height [m]
h_m	local convective mass transfer coefficient [m/s]
$\overline{h}_m$	average convective mass transfer coefficient along the walls [m/s]
I	identity matrix
J	Jacobian matrices

k	molecular thermal conductivity [W/mK]
k_T	turbulent thermal conductivity [W/mK]
k_e	effective thermal conductivity [W/mK]
L	channel length [m]
L_x, L_y	left hand side operators
$\dot{m}$	mass flow [kg/s]
M	time step
No''_w	mass flux of the chemical species at the walls [kg/m^{2}s]
$\overline{p}_e$	mean effective pressure [Pa]
Pr_T	turbulent Prandtl number [-]
Q	vector of conserved variables
R_x, R_y	right hand side operators
Re_{Dh}	Reynolds number based on the hydraulic diameter [-]
S	step height [m]
S	source term
Sc	molecular Schmidt number [-]
Sc_T	turbulent Schmidt number [-]
Sh	Sherwood number [-]
$\overline{Sh}$	average Sherwood number along the channel length [-]
t	time [s]
$\overline{T}$	average temperature [K]
T_i	inlet temperature [K]
u^*	shear velocity [m/s]
$\overline{u}_i$	Cartesian components of the average velocity [m/s]
u_i	inlet velocity [m/s]
u_m	mean velocity in the channel cross section [m/s]
x_i	Cartesian axis [m]
y^+	non-dimensional distance from the wall [-]

Greek Letters

$\sigma_k, \sigma_\varepsilon$	turbulence model constants [-]
κ	turbulent kinetic energy [m^2/s^2]
κ_i	turbulent kinetic energy at the inlet [m^2/s^2]
ε	dissipation rate [m^2/s^3]
$\varepsilon_i, \varepsilon_e$	coefficients of artificial dissipation [-]
μ	dynamic viscosity [kg/ ms]
μ_T	eddy viscosity [kg/ms]
μ_e	effective viscosity [kg/ms]
ρ	density [kg/m^3]

Subscripts

e	effective quantity
i	inlet section and vector subscript
m	average quantity
T	turbulent quantity

REFERENCES

Arellano, J. S., Xáman, J., Álvarez, G. and Rivera, M. G., Heat and mass transfer by natural convection in a square cavity filled with mixture of air-CO_2. International Journal of Heat and Mass Transfer, 64, p. 725 (2013).

Arellano, J. S. and Rivera, M. G., Conjugate heat and mass transfer by natural convection in a square cavity filled with mixture of air-CO_2. International Journal of Heat and Mass Transfer, 70, p. 103 (2014).

Arpaci, V. S., and Larsen, P. S., Convection Heat Transfer. Prentice-Hall Inc., New Jersey (1984).

Beam, R. M. and Warming, R. F., An implicit factored scheme for the compressible Navier-Stokes equations. AIAA Journal, 16, p. 393 (1978).

Incropera, F. P., Witt, D. P., Bergman, T. L. and Lavine, A. S., Fundamentals of Heat and Mass Transfer. John Wiley & Sons, Inc., New Jersey (2007).

Kadem, S., Lachement, A., Younsi, R. and Kocaefe, D., 3d-Transient modeling of heat and mass transfer during heat treatment of wood. International Communications in Heat and Mass Transfer, 38, p. 717 (2011).

Kader, B. A., Temperature and concentration profiles in fully turbulent boundary layers. International Journal of Heat and Mass Transfer, 24, p. 1541 (1981).

Kays, W. M. and Crawford, M. E., Convective Heat and Mass Transfer. McGraw Hill Inc., New York (2005).

Launder, B. E. and Spalding, D. B., The numerical computation of turbulent flows. Computer Methods in Applied Mechanics and Engineering, 3, p. 269 (1974).

Lamnatou, C., Papanicolaou, E., Belessiotis, V. and Kyriakis, N., Conjugate heat and mass transfer from a drying rectangular cylinder in confined air flow. Numerical Heat Transfer, Part A, 56, p. 379 (2009).

Lateb, M., Masson, C., Stathopoulos, T. and Bédard, C., Comparison of various types of $\kappa - \varepsilon$ models for pollutant emissions around a two-building configuration. Journal of Wind Engineering and Industrial Aerodynamics, 115, p. 9 (2013).

Mohan, V. P. C. and Talukdar, P., Three dimensional numerical modeling of simultaneous heat and

moisture transfer in a moist object subjected to convective drying, International Journal of Heat and Mass Transfer, 53, p. 4638 (2010).

Patankar, S. V., Numerical Heat Transfer and Fluid Flow. Hemisphere Pub. Co., New York (1980).

Possamai, D. G., Análise numérica do escoamento turbulento no interior de secadores Dissertação de Mestrado, CCT - UDESC, Joinville (2013). (In Portuguese).

Vaz Jr, M., Zdanski, P. S. B., Cerqueira, R. F. L. and Possamai, D. G., Conjugated heat and mass transfer in convective drying in compact wood kilns: A system approach. Advances in Mechanical Engineering, 2013, p. 1 (2013).

Xiong, J., Cheng, X., and Yang, Y., Numerical investigation on mass transfer enhancement downstream of an orifice. International Journal of Heat and Mass Transfer, 68, p. 366 (2014).

Younsi, R., Kocaefe, D., Poncsak, S., and Kocaefe, Y., Computational and experimental analysis of high temperature thermal treatment of wood based on ThermoWood technology. International Communications in Heat and Mass Transfer, 37, p. 21 (2010).

Zdanski, P. S. B., Ortega, M. A. and Fico Júnior, N. G. C. R., Numerical simulation of the incompressible Navier-Stokes equations. Numerical Heat Transfer, Part B, 46, p. 549 (2004).

Zdanski, P. S. B., Vaz Jr, M. and Inácio, G. R., A finite volume approach to simulation of polymer melt flow in channels. Engineering Computations, 25, p. 233 (2008).

Zdanski, P. S. B. and Vaz Jr, M., A numerical method for simulation of incompressible three-dimensional Newtonian and non-Newtonian flows. Numerical Heat Transfer, Part B, 59, p. 360 (2011).

Zdanski, P. S. B., Possamai, D. G. and Vaz Jr, M., A numerical assessment of the air flow behavior in a convectional compact dry kiln. Journal of Applied Fluid Mechanics, 8, p. 367 (2015).

Zdanski, P. S. B., Vaz Jr, M. and Gargioni, G. T., Convection heat transfer enhancement on recirculating flows in a backward facing step: The effects of a small square turbulence promoter. Heat Transfer Engineering, 37, p. 162 (2016).